Photocrosslinkable Chitosan–Nanocellulose Composite Hydrogels for Hemostatic, Antibacterial, and Soft-Tissue Biomedical Applications

Jhaleh Amirian [*,†], Ehsan Amel Zendehdel [†], Antons Sizovs, Ingus Skadiņš, Agnese Brangule [*], Dace Bandere [*]

Posted Date: 13 March 2026

doi: 10.20944/preprints202603.1038.v1

Keywords: oxidized cellulose nanofiber (OCNF); chitosan methacrylate (ChiMA); composite hydrogel; hydrogel ink; wound healing

 doi:10.20944/preprints202603.1038.v1

Article

Photocrosslinkable Chitosan–Nanocellulose Composite Hydrogels for Hemostatic, Antibacterial, and Soft-Tissue Biomedical Applications

Jhaleh Amirian [1,2,*,†], Ehsan Amel Zendehdel [3,†], Antons Sizovs [2,4], Ingus Skadiņš [2,5], Agnese Brangule [1,2,*] and Dace Bandere [1,2,*]

[1] Riga Stradins University, Department of Pharmaceutical Chemistry, Riga LV-1007, Latvia
[2] Baltic Biomaterials Centre of Excellence, Headquarters at RigaTechnical University, Riga LV-1048, Latvia
[3] The Faculty of Art and Architecture, Eshragh Institute of Higher Education, F8FQ+9V3 Bojnord, Iran
[4] Laboratory of Pharmaceutical Pharmacology, Latvian Institute of Organic Synthesis, Riga LV-1006, Latvia
[5] Department of Biology and Microbiology, Riga Stradiņš University, Riga LV-1007, Latvia
* Correspondence: jalehamirian@gmail.com or amirianj@tcd.ie (J.A.); agnese.brangule@rsu.lv (A.B.); dace.bandere@rsu.lv (D.B.)
† These two author contibuted equally.

Abstract

Bleeding and bacterial infection remain major challenges in surgical procedures. Thus, hemostatic biomaterials capable of controlling bleeding rapidly while preventing microbial contamination are highly desirable. This study developed and evaluated photocrosslinkable composite hydrogels made of methacrylated chitosan (ChiMA) and methacrylated oxidized cellulose nanofibers (OCNFMA) for antibacterial hemostatic applications. Chitosan (Chi) was methacrylated using methacrylic anhydride, cellulose nanofibers were oxidized with sodium periodate, and 2-aminoethyl methacrylate (AEMA) was added to introduce photocrosslinkable groups. For the preparation of composite hydrogel networks, the precursor solutions were mixed and photocrosslinked under UV irradiation (365 nm) in the presence of lithium phenyl-2,4,6-trimethylbenzoylphosphinate (LAP). A Fourier transform infrared spectrometer (FTIR), scanning electron microscope (SEM), and rheological analysis were utilized to characterize the materials. Hydrogels were evaluated for swelling behavior, degradation profile, and blood clotting ability. Furthermore, antibacterial activity against Staphylococcus aureus (SA) and Pseudomonas aeruginosa (PA) was evaluated, and cytocompatibility was evaluated using NIH3T3 fibroblasts and MC3T3 preosteoblasts. Incorporating OCNFMA with low degrees of functionalization (L) or high degrees of functionalization (H) at different ratios into the ChiMA network significantly influenced the physicochemical and structural properties of the hydrogels. The composite hydrogels exhibited interconnected porous structures, improved mechanical stability, and tunable swelling and degradation behavior. Furthermore, some formulations demonstrated measurable antibacterial activity against both bacterial strains. Moreover, cytocompatibility studies revealed that the composite hydrogels supported higher cell viability than ChiMA alone. The developed ChiMA–OCNFMA composite hydrogels exhibit promising physicochemical, antibacterial, and biological properties. The findings suggest that the materials may be useful as multifunctional hydrogels for wound management, as well as candidates for broader biomedical applications.

Keywords: oxidized cellulose nanofiber (OCNF); chitosan methacrylate (ChiMA); composite hydrogel; hydrogel ink; wound healing

 doi:10.20944/preprints202603.1038.v1

1. Introduction

Bleeding following surgical procedures, traumatic injuries, or similar clinical conditions remains a significant challenge for surgeons [1–4]. Local hemostatic agents are considered the first-line treatment for various types of bleeding, particularly when suturing, direct compression, or electrocautery are contraindicated or impractical [1,2,4]. The ideal hemostatic agent should provide rapid bleeding control, exhibit biocompatibility and biodegradability, possess antibacterial properties, and be easy to apply and cost-effective [2,4].

The hydrogels are a class of biomaterials that can be applied directly to wound sites in order to control bleeding [1,5]. A number of advantages have been attributed to these materials in this context, such as high water content, tissue-like mechanical compliance, injectability, and moldability [1,6]. Further, hydrogels can undergo in situ crosslinking through mechanisms such as enzymatic reactions [7,8], photocrosslinking[5,9,10], or chemical reactions such as Schiff-base formation[1,11], enabling them to quickly form stable networks at the application site[2,5]. Healing chronic wounds is complex and long, which is often complicated by bacterial infections [12]. When microbial colonization persists, it disrupts the normal stages of wound healing inculding hemostasis, inflammation, proliferation, remodeling which resulted in delayed tissue regeneration and greater risk of complications. There are a number of microorganisms that can cause chronic wound infections, but two pathogens are especially prevalent: Staphylococcus aureus (SA) and Pseudomonas aeruginosa (PA) [12]. SA is a Gram-positive bacterium commonly found on the skin and mucosa. While it is commonly present as part of the normal microbiota, it can easily penetrate damaged tissue and cause a variety of infections ranging from superficial skin lesions to severe systemic conditions [13]. Its ability to spread through the body, infecting skin, mucous membranes, and the gastrointestinal tract while also causing severe, life-threatening disease, highlights its clinical complexity [13]. Conversely, PA is a Gram-negative opportunistic pathogen that is frequently detected in chronic wounds and wounds that are not healing [14]. There are several concerns associated with PA, including its strong ability to form biofilms, its intrinsic antibiotic resistance mechanisms, and its ability to secrete toxins that can cause tissue damage to the host[14]. Therefore, inflammation and delayed healing are strongly associated with PA contamination in wound sites [14].

Polysaccharide-based hydrogels such as chitosan, cellulose, hyaluronate, and carrageenan have received a lot of attention in wound healing and other biomedical applications inculding bulinking agents for urienry inconteience[1]. Chitosan is a natural biopolymer that is made by deacetylating natural chitin. It has demonstrated biocompatibility and biodegradability, making it one of the most promising polysaccharide materials for wound healing[1]. Besides its amino groups, chitosan also contains abundant hydroxyl groups along its polysaccharide backbone [15]. The presence of both amino and hydroxyl functional groups allows for multiple reactive sites, making chitosan a highly versatile biopolymer for chemical modification and cross-linking [1,15]. Similarly, cellulose nanofibers (CNFs), which are typically obtained from wood pulp, consist of 1-linked glucose units containing a high density of hydroxyl groups (-OH) [16,17]. A high density of hydroxyl groups on the surface of cellulose nanofibers (CNFs) contributes to their hydrophilicity and provides a wide range of possibilities for chemical modification[18]. Through treatment with sodium periodate, these groups can undergo oxidation, resulting in aldehyde functionalities [19]. Additionally, the hydroxyl functional group in CNF enables extensive hydrogen bonding between the polymer and other polymers, contributing to the formation and stabilization of hydrogel networks through second networks and physical crosslinking [20].

By chemically modifying their functional groups, both chitosan and cellulose nanofibers can be further tailored to meet individual needs [5,9,20]. The hydroxyl groups present on CNFs can be oxidized and subsequently conjugated with reactive methacrylation agents [19], while the primary amino groups in chitosan can directly react with methacrylic anhydride (MA) [21] or other methacrylate-containing reagents to introduce methacrylate functionalities along the polymer backbone. The incorporation of methacrylate groups enables the formation of polymers that are photo- or radical-crosslinkable[5,21,22]. Thus, these modified polysaccharides can be converted from

 doi:10.20944/preprints202603.1038.v1

a liquid precursor (sol) to a crosslinked hydrogel network upon exposure to light [21,22]. Multiple methcaylation agents are available, including MA and 2-aminoethyl methacrylate (AEMA), 2-isocyanatoethyl methacrylate (IEM) and glycidyl methacrylate (GM) [5,9]. Depending on the available functional groups, polysaccharides can be modified using methacrylation agents[5,9,21,22].

Here, we present the development of photocrosslinkable composite hydrogels consisting of methacrylated chitosan (ChiMA) and methacrylated oxidized cellulose nanofibers (OCNFMA). Upon exposure to UV irradiation in the presence of LAP, the precursor solutions were rapidly crosslinked to form stable hydrogel networks. These hydrogels were evaluated for their physicochemical properties, blood clotting capability, antibacterial activity, and cytocompatibility, with promising results for hemostatic wound management and future use as soft tissue fillers.

2. Materials and Methods

2.1. Chemical

Chitosan (Chi, medium molecular weight, Sigma-Aldrich), sodium periodate (NaIO4, > 99.0%, Fisher Scientific), 2-Aminoethyl methacrylate hydrochloride (AEMA, ≥ 90%, Sigma-Aldrich), ethylene glycol (99.5%, ITW Reagents), methacrylic anhydride (MA, >94%, Sigma-Aldrich), ammonium hydroxide (NH_4OH, ≥25%, Sigma-Aldrich) and cellulose nanofiber (OXILVA, Norway) were purchased and used as-received.

NIH 3T3 cells obtained from the American Type Culture Collection (ATCC®, USA) were used for in vitro studies. For in vitro studies, Dulbecco's modified Eagle's medium (DMEM), fetal bovine serum (FBS, Gibco, Thermo Fisher Scientific), penicillin-streptomycin (PS, Gibco, Thermo Fisher Scientific), phosphate-buffered saline 1x (PBS, Gibco, Thermo Fisher Scientific), isopropyl alcohol (Sigma-Aldrich), and MTT (3-(4,5-dimethylthiazol-2-yl)-2,5-diphenyltetrazolium bromide) (BLD Pharmatech LTD, Shanghai, China) were purchased and used as received.

2.2. Method

2.2.1. Cellulose Nanofiber (CNF) Functionalization

Oxidized cellulose nanofiber (ONCF) was synthesized based on previous studies with minor modifications. The oxidation of the cellulose nanofibers (CNF) was carried out on two different levels. Sodium periodate, in quantities of 0.25 g and 0.5 g, was dissolved in 5 mL of distilled water and subsequently added to 25 mL of CNF suspension with a 2 wt.% concentration and stirred at room temperature for 24 hours. To stop the reaction, 1-2 ml of ethylene glycol was added to each bottle, and the solutions were then separately poured into a dialysis tube with a 3,500 kDa cut-off and dialyzed for 5 days. The remaining IO_3 in the dialysis water was tested using the $AgNO_3$ test. This process results in the production of low-oxidized cellulose nanofibers (OCNF-L) and high-oxidized cellulose nanofibers (OCNF-H), respectively.

Following purification by dialysis, the solution was transferred to a 50 mL bottle, and AEMA was added in amounts of 0.4 g and 0.8 g to the L-OCNFMA and H-OCNFMA solutions, respectively, to produce OCNFMA hydrogels with low (OCNFMA-L) and high (OCNFMA-H) levels of methacrylation. The solutions were stirred overnight at room temperature and then transferred to dialysis tubes with a 3500 kDa molecular weight cut-off. Dialysis was conducted for ten days, and the water was changed two to three times each day. The solid content of the solution was determined by placing a sample of 1 mL in a pre-weighed container and drying the sample at 37 °C for 24 hours. The solution was concentrated in dialysis tubing, and the resulting concentration and wieght percentage was subsequently measured.

2.2.2. Chitosan Methacrylation

In accordance with the methodology previously established in the literature, we conducted the methacrylation of chitosan. For this purpose, 2.5 g of chitosan were dissolved in 200 mL of an acetic acid solution containing 2% v/v acetic acid to create a solution containing 1.25% chitosan [23]. Upon

 doi:10.20944/preprints202603.1038.v1

the dissolution of the chitosan, 12 grams of methacrylate anhydride were introduced into the solution. Following this, the mixture was stirred overnight at 60 °C [23]. Ammonia was used to bring the pH level down to 6 ± 0.2 once the mixture had cooled to room temperature [23]. The solution was then dialyzed for 7 days against deionized water (DI). The solution was frozen at -80 °C for 4–8 hours and subsequently lyophilized for four days, yielding 1.5 grams of ChiMA, a white, porous, and water-soluble solid.

2.2.3. ChiMA-OCNFMA Composite Hydrogel Prepration

According to **Table 1**, ChiMA, ChiMA-OCNFMA-L, and ChiMA-OCNFMA-H hydrogels were prepared based on their mass ratios (wt.%). In order to prepare ChiMA, a solution of ChiMA at a concentration of 1 wt.% was first prepared and subsequently mixed with LAP at a concentration of 0.4 wt.% at room temperature. Composite hydrogels with low and high methacrylation, including ChiMA7-OCNFMA3, ChiMA5-OCNFMA5, and ChiMA3-OCNFMA7, were prepared by mixing a ChiMA solution at 1 wt.% with LAP, followed by adding OCNFMA-L and OCNFMA-H at varying concentrations (Table 1). Following this, the solution was thoroughly mixed in a vortex mixer. To examine the properties of photocrosslinked hydrogels, the desired hydrogel solution was poured into PDMS molds with dimensions of (well size 10 mm × 4 mm) and UV irradiated for 3 min at 7 mW/cm^2.

Table 1. Composition of ChiMA–OCNFMA hydrogel formulations.

Sample name	ChiMA (wt.%)	OCNFMA (wt.%)	Title 3
ChiMA	100	0	-----
ChiMA7–OCNFMA3–L	70	30	Low methacrylation (L)
ChiMA5–OCNFMA5–L	50	50	Low methacrylation (L)
ChiMA3–OCNFMA7–L	30	70	Low methacrylation (L)
ChiMA7–OCNFMA3–H	70	30	High methacrylation (H)
ChiMA5–OCNFMA5–H	50	50	High methacrylation (H)
ChiMA3–OCNFMA7–H	30	70	High methacrylation (H)

2.3. Characterization

2.3.1. Scanning Electron Microscopy (SEM)

The surface morphology of the ChiMA, and ChiMA-OCNFMA was imaged using a scanning electron microscope (FESEM, MIRA3 FEG-SEM, Tescan, Brno, Czech Republic) operated at an accelerating voltage of 2 kV. Samples were transferred to the SEM holder and sputtered with carbon nanotubes in a 15-pulse mode. In order to carry out the SEM analysis of the CNF, OCNF-L, OCNF-H, OCNFMA-L, and OCNFMA-H, a small quantity of samples was dispersed in water and subjected to sonication. Subsequently, the resultant suspension was deposited onto an aluminum substrate and allowed to undergo the natural drying process in room temperature.

2.3.2. Fourier Transform Infrared (FTIR) Spectroscopy

The Fourier transform infrared (FTIR) analysis was carried out within the wavenumber range of 400 cm^{-1} to 4000 cm^{-1} on a Nicolet iS50 spectrometer (Thermo Fisher Scientific, USA), with a resolution of 4 cm^{-1} and 64 scans appended for each sample. An air background spectrum was obtained before collecting sample spectra.

2.3.4. Rheology

The rheological assessments were performed on the MCR302 rheometer, which is manufactured by Anton Paar. To obtain amplitude sweeps, a parallel plate geometry with a 25 mm diameter top

 doi:10.20944/preprints202603.1038.v1

plate and a 2 mm gap in the oscillatory settings was used. The hydrogel samples were subjected to photocrosslinking within a mold with dimensions of 35 mm in diameter and 2 mm in height for 3 min, following which they were loaded onto the parallel-plate geometry. All the measurements were carried out at a temperature of 37 °C. A constant frequency of 1 Hz was used to conduct amplitude sweeps in an oscillatory mode, with the strain increasing from 0.01 to 10%. The stiffness of the hydrogel was ascertained at a frequency of 1 Hz and 0.2% strain, which fell within the linear viscoelastic region (LVR).

2.3.5. Swelling Behavior and Weight Loss

To assess the swelling behavior, preweighed, freeze-dried ChiMA1 and ChiMA-OCNFMA hydrogels were dipped in PBS at 37 °C for 1, 2, 3, 4, 8, 24, and 48 hours to evaluate the hydrogels' swelling behavior. Initially, the hydrogels were placed in 24-well plates containing 2 ml of PBS to allow for swelling. After the swelling process, the hydrogels were carefully removed and placed on filter paper to absorb any excess water. The weight of the swollen hydrogels (Wt) was then recorded at predetermined time intervals. The swelling percentage was calculated using Equation (1) (Eq. 1)

$$Sweeling\ ratio\% = (Wt - W0/W0) * 100 \text{ Eq1}$$

Throughout the experiment, W0 represents the initial weight of the hydrogel, and Wt represents the weight of the swelled hydrogel at each time point.

As part of our evaluation of hydrogel degradation and weight loss, we used the ASTM F1635-16 protocol and other studies conducted by us. The weight of hydrogels was measured over time at intervals of 0.3, 7, 10, 14, 21, 28, 35, 42, and 49 days in order to evaluate how the hydrogels degraded. Based on Equation (2) (Eq. 2), the weight loss of the hydrogel was calculated.

Degradation %= (W0 −Wt/ W0)*100 Eq2

where W0 represents the initial weight of the hydrogel and Wt represents its weight during each specified period.

2.4. Blood Clotting Index (BCI) and Red Blood Cells (RBC) Attachment on Scaffolds

Based on previous studies, an evaluation of blood clotting was carried out [24]. These experiments were conducted on samples of 8 mm x 2 mm in dimension. To prepare the recasified whole blood solution, 8 µL of calcium chloride in 0.2 M concentration were added to 100 µL of fresh blood. After incubation for 30 minutes at 37 °C, 25 µL of recalcified whole blood were placed on the hydrogel. Following that, samples were incubated for 60, 90, 120, and 150 seconds, respectively. In this study, glass dishes without samples and gauze were used as positive and negative controls, respectively. Upon completion of the defined time interval, 5 mL of the DI water was gently added to the glass bottle without disturbing the attached clots. Afterwards, the supernatent was collected and kept at 37 °C for 1 hour; then, the absorbance of the 200 µL of supernatent was measured using a microplate reader at 540 nm. In order to calculate the BCI, the following equation was used

BCI %= (Is −I0/ Is −I0)*100

, in which Is represents the absorbance of the samples or the positive control, and I0 represents the absorbance of the negative control.

The red blood adhesion test was conducted in accordance with previous references. The samples were initially incubated in DPBS for one hour at 37 C. After the PBS solution was removed from the hydrogel, fresh blood was added dropwise to the hydrogel and incubated for five minutes. To prepare the samples for SEM imaging, the samples were washed two times with DPBS for 5 min each to remove unattached blood cells from the hydrogel samples and then fixed with formaldehyde 2.5%. After that, samples were washed twice with PBS and then dehydrated with ethanol solution series 50%, 60%, 70%, 80%, 90%, 95%, and 100% each. The samples were then analyzed by SEM.

 doi:10.20944/preprints202603.1038.v1

2.5. Antibacterial Properties

The antibacterial activity of the ChiMA and ChiMA–OCNFMA hydrogels was checked using the agar disk diffusion method. Two bacterial strains were selected: Gram-positive Staphylococcus aureus and Gram-negative Pseudomonas aeruginosa. Nutrient agar was prepared by 14 g of nutrient agar being dissolved in 500 mL of deionized water, followed by sterilisation by autoclaving at 121 °C for 20 min. The agar solution, which had been sterilised, was poured into sterile Petri dishes (10 cm diameter) and left to solidify. The agar surface was evenly spread with fresh bacterial suspensions using sterile cotton swabs. Hydrogel samples with identical dimensions were aseptically placed on the inoculated agar plates. The plates were left to incubate at 37 °C for 24 hours. Then, the diameters of the inhibition zones around the samples were measured to evaluate the antibacterial activity. Plates without hydrogel samples served as negative controls. All experiments were conducted in triplicate.

2.6. Cell Cultivation and Cytotoxicity Measurements by Lived Dead Assay for Leachable

The cytotoxicity of the ChiMA and ChiMA-OCNFMA hydrogels was determined using two cell lines, NIH3T3 (CRL-1658TM, ATCC) and MC3T3 (ATCC). NIH3T3 cells were cultured in DMEM (Sigma) containing 10% fetal calf serum (FCS) and 100 µg/mL of penicillin at 37 C and MC3T3 cells were cultured in α-MEM with 10% fetal bovine serum (FBS) at 37 C. As part of the indirect contact cytotoxicity testing, 200 mg of the freeze-dried scaffold was immersed in 1.3 mL of DMEM for NIH3T3 cells and α-MEM for MC3T3 cells, both for 24 hours at 37 °C. In the following step, supernatants were aspirated, and FSC and FBS were added to a final concentration of 10%. NIH3T3 cells or MC3T3 cells were seeded in 96-well plates (N=6) and incubated in 100 µL of complete medium (DMEM with 10% FCS for NIH3T3 and α-MEM with FBS for MC3T3). Upon completion of 24 hours of incubation, the medium was removed and replaced with 100 µL of materials extracts. The cells were then incubated for an additional 24 hours. Following 24 hours of incubation, calcein-AM and propidium iodide were used according to the manufacturer's instructions for performing a live-dead assay. The results were analyzed using a one-way ANOVA followed by Dunnett's multiple comparison test.

Dual-Syringe Design and 3D Design

A custom dual-syringe extrusion device was designed using SOLIDWORKS 2021 (Dassault Systèmes, France) to enable simultaneous delivery and mixing of the hydrogel precursor solutions. The 3D model was exported in STL format for additive manufacturing. The prototype was created using fused deposition modelling (FDM) with a Bambu Lab P1S desktop 3D printer (Bambu Lab, Shenzhen, China). The slicing software Bambu Studio was used to process the STL file, in order to generate the printing parameters and toolpaths.

The printing was done using a 1.75 mm diameter polylactic acid (PLA) filament. The main printing parameters included a 0.4 mm nozzle diameter, 0.2 mm layer height, nozzle temperature of 200–210 °C, build plate temperature of 55–60 °C, 20–30% infill density, and a printing speed of 50–100 mm s^{-1}, providing adequate dimensional accuracy and mechanical stability of the printed components. After printing, the components were removed from the build plate and post-processing steps were performed, including support removal and surface cleaning. The printed parts were then put together to make the final dual-syringe device. PLA was selected as the printing material due to its ease of fabrication, dimensional stability and suitability for rapid prototyping of functional laboratory devices.

The device was designed to hold two standard 5 ml disposable syringes in parallel within the printed holder. The system is equipped with an optical illumination module that enables localized photocrosslinking. The UV LED (3 W, 395 – 400 nm) was mounted on an aluminum heat sink to provide excitation. UV light was guided through a 2 mm plastic optical fiber to the needle tip, allowing localized delivery to the extrusion region. This illumination module was powered by a 12 V DC supply using an MT3608 DC–DC boost converter for voltage regulation, and it was controlled

 doi:10.20944/preprints202603.1038.v1

by a manual on/off switch. During the extrusion process, this configuration enabled efficient UV delivery and in situ photocrosslinking of the hydrogel.

During operation, the ChiMA/LAP solution and the OCNFMA dispersion were loaded separately into each syringe. Homogeneous mixing prior to deposition was enabled through simultaneous delivery of the solutions via a static mixing nozzle during manual extrusion. The material was extruded directly onto the substrate and then photocrosslinked under UV LED irradation (3 W, 395 – 400 nm) to form stable hydrogel structures. The custom dual-syringe system enabled controlled extrusion, homogeneous mixing of the precursor solutions, and convenient handling during hydrogel injection at the intended implantation site.

3. Results

Scheme 1 schematically illustrates the oxidation of CNF to OCNF, the methacrylation of OCNF via AEMA, and the methacrylation of chtosan via MA. **Scheme 1A,B** show the preparation of OCNFMA, begins with the oxidation of CNF using sodium periodate ($NaIO_4$) to form aldehyde groups. These aldehydes then react with the amine in AEMA through a Schiff-base reaction, completing the modification process. Meanwhile, ChiMA is prepared from chitosan through nucleophilic addition, where the carboxyl group of MA reacts with the amine group of chitosan, introducing methacrylate functionality. **Scheme 1C** illustrates the UV-induced crosslinking of ChiMA and OCNFMA-ChiMA using LAP as a photoinitiator, forming a stable hydrogel. The reaction occurs between the methacrylate groups on ChiMA and OCNFMA, enabling covalent bonding.

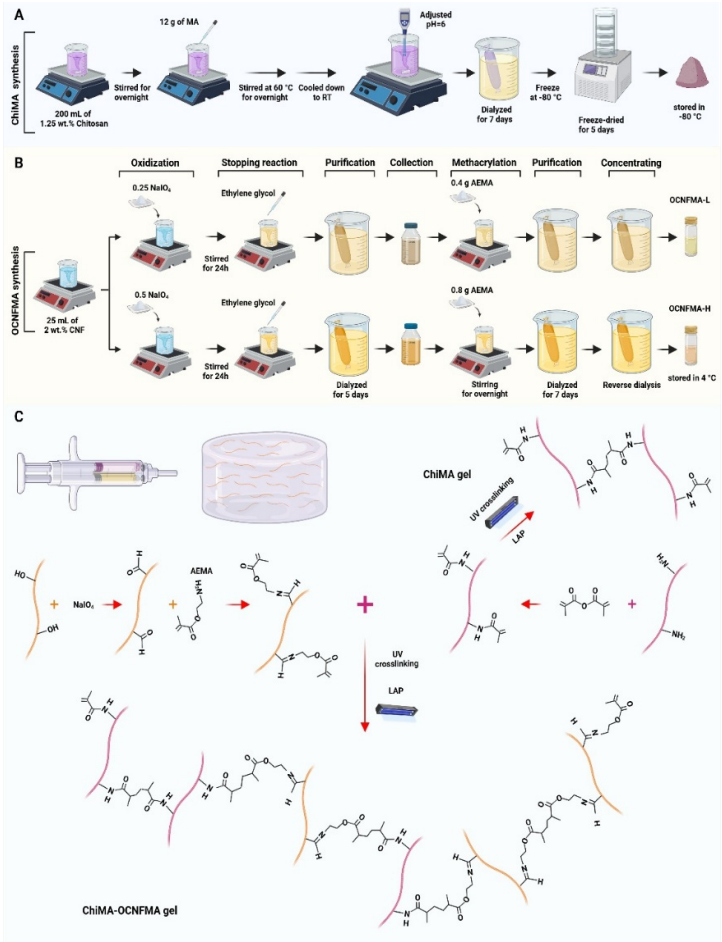

Scheme 1. Overview of functionalization of chitosan and CNF, including (A) methacrylation of chitosan with MA, (B) The oxidation of CNF by sodium periodate and its methacrylation by AEMA, as well as the purification

 doi:10.20944/preprints202603.1038.v1

of ONFMA and concentrating of OCNFMA, (C) Production of photocrosslinked ChiMA and ChiMA-OCNFMA gels through photocrosslinking in the presence of LAP under 365 nm irradiation.

Figure 1A,B show the FTIR spectra of Chi and CNF, highlighting the chemical modifications applied to each. Chitosan was modified by methacrylating with MA, while CNF was oxidized and then methacrylated using AEMA. FTIR spectrum of ChiMA is shown in Figure 1A. It shows distinct absorption bands at 1315, 1400, and 1600 cm-1, which are attributed to C=O stretching (amide III), N-H bending and C-N stretching (amide II), and amide I vibrations, and together indicate the successful introduction of methacrylate groups. Figure 1B shows FTIR spectra of CNF, OCNF, and OCNFMA. Upon oxidation with sodium periodate, the spectrum of OCNF shows a new peak at about 1700 cm-1, which is attributed to the C=O stretching of the aldehyde groups, and a band at about 1620 cm-1, corresponding the asymmetric stretching of the aldehyde-related vibrations. These peaks are not present in the unmodified CNF spectrum, which confirms the successful introduction of the aldehyde functionality. The OCNF-H sample exhibits stronger absorption in these regions, indicating a higher oxidation level. Furthermore, the appearance of a band near 815 cm-1 in the OCNFMA spectrum is assigned to =C-H out-of-plane bending vibrations, which confirms the successful methacrylation. A distinct peak around 1635 cm-1, along with another around 815 cm-1 in the OCNFMA spectrum, indicates the presence of vinyl groups. These signals are indicative of the successful grafting of methacrylate groups, indicating that the cellulose nanofibers were effectively modified in accordance with the design intent. Figure 1C,D illustrate the FTIR spectra of composite hydrogels formed by combining ChiMA with OCNFM at different oxidation and methcrylation levels. Three composite formulations with ChiMA:OCNFM ratios of 7:3, 5:5 and 3:7 were prepared for both OCNFM-L and OCNFM-H. All samples show characteristic peaks of both ChiMA and OCNFA, confirming the successful composite network formed. Furtgermore, FTIR spectra show that composites containing OCNFM-H have higher absorption intensities than those containing OCNFM-L, indicating stronger interactions or higher crosslinking.

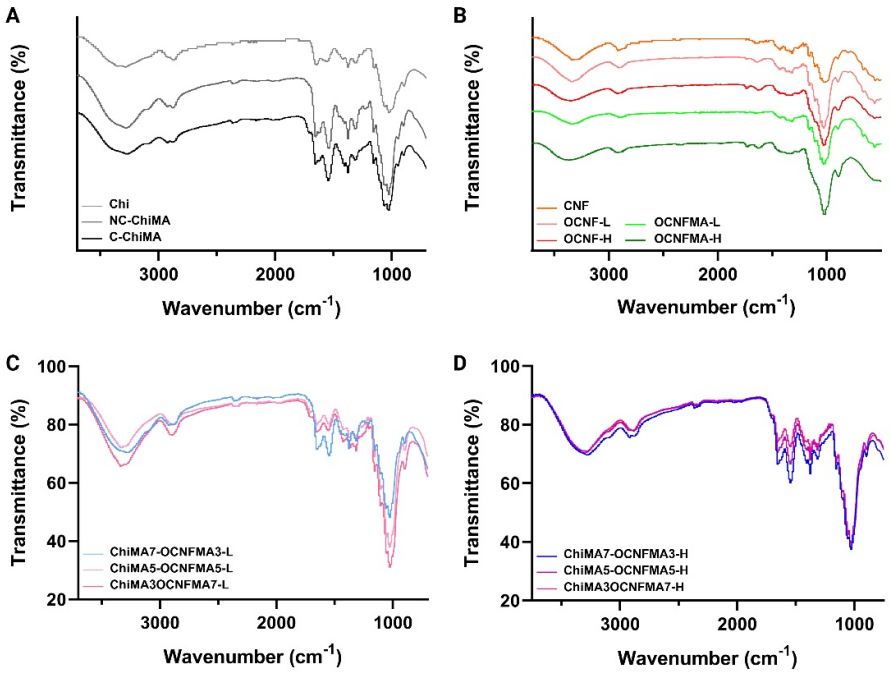

Figure 1. (A) Spectra of chitosan (Chi), NC-ChiMA, and C-ChiMA. (B) Spectra of CNF and OCNF, and OCNFMA with low (L) and high (H) oxidation levels and low (L) and high (H) methacrylation levels. (C, D) Spectra of ChiMA-OCNFMA composites incorporating OCNFM-L and OCNFM-H at different ChiMA:OCNFMA weight ratios (7:3, 5:5, and 3:7), respectively.

 doi:10.20944/preprints202603.1038.v1

SEM images of CNF before and after oxidation with sodium periodate and methacrylation with AEMA are shown in Figure 2A. Before modification, CNF shows a dense and smooth fibrous network containing thin, tightly entangled nanofibers. Upon modification, the fibers undergo noticeable changes in both structure and thickness. In comparison with the unmodified samples, OCNFMA-L exhibits a slight increase in fiber thickness, whereas OCNFMA-H exhibits noticeably thicker fibers. Based on these results, it appears that greater degrees of oxidation and methacrylation result in increased fiber thickness and enhanced entanglement, likely due to greater surface functionalization. This morphological evolution may enhance the material's reactivity and suitability for forming well-integrated composite hydrogel materials.

Figure 2B shows the SEM image of the ChiMA and ChiMA-OCNFMA composites with incorportaing various OCNFM-(H) at different ChiMA:OCNFMA weight ratios (7:3, 5:5, and 3:7). SEM images of the surface and cross-sectional morphology of ChiMA indicate that it has a porous morphology with relatively large and interconnected pores. The images also demonstrate that ChiMA:OCNFM-L composites have larger pores than ChiMA:OCNFM-H. The difference may be attributed to the low methacrylation content of ChiMA:OCNFM-L, which results in lower crosslinking density and a less compact network structure. An interconnected pore structure suggests that the scaffold can facilitate efficient nutrient exchange, which is essential to the infiltration and growth of cells.

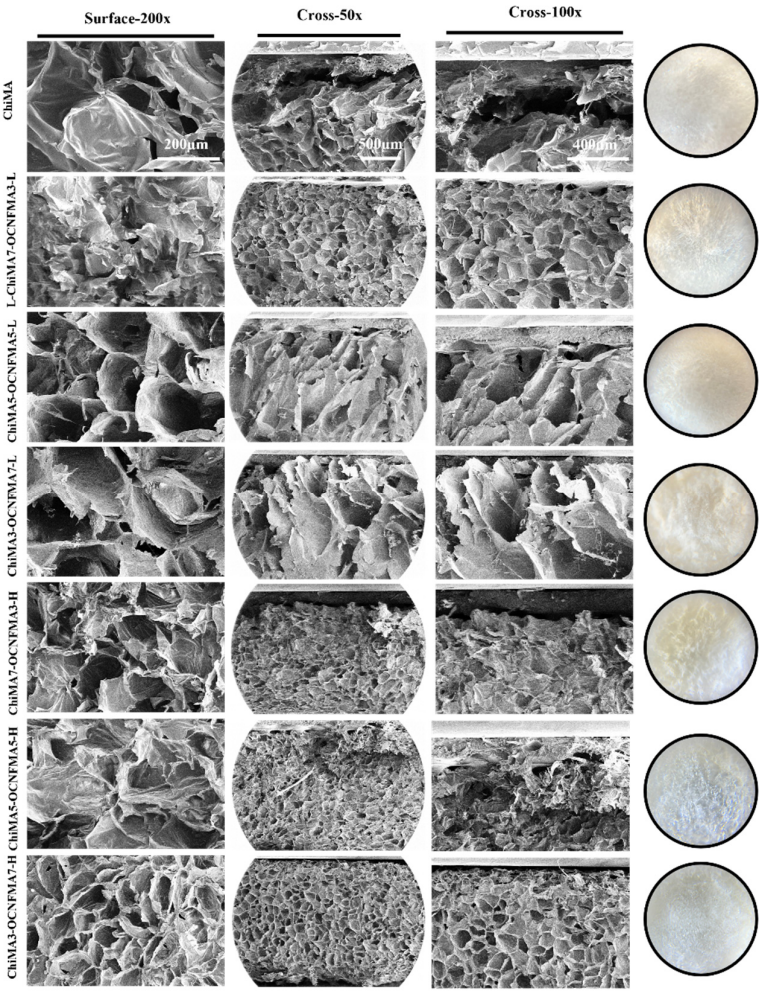

Figure 2. SEM images of ChiMA-based composite hydrogels and ChiMA-OCNFMA composite hydrogels with different formulations. Surface morphology is shown at 200× magnification and cross-sectional views at 50× and 100× magnification. Samples include different ChiMA:OCNFMA ratios (7:3, 5:5, 3:7) with both low (L) and high

 doi:10.20944/preprints202603.1038.v1

(H) levels of oxidation and methacrylation. Macroscopic views of the lyophilized hydrogels are shown on the right.

All hydrogel formulations, including ChiMA and its composites with OCNFMA-L and OCNFMA-H functionalisation at 7:3, 5:5, and 3:7 weight ratios, were tested for amplitude sweep (Figure 3A). In all samples, the storage modulus (G′) was consistently higher than the loss modulus (G″) over the applied strain range, indicating a predominantly elastic and solid-like behavior for the hydrogel networks. Incorporating OCNFMA had a significant impact on the mechanical properties of the hydrogels, depending on the level of functionalization and composition. There was no significant change in the crossover point (G′ = G″) in composites containing OCNFMA-(L), which was similar to that of pure ChiMA. In contrast, hydrogels containing OCNFMA-(H) showed a slight shift in crossover strain, suggesting modifications in network stability and crosslink density. Figure 3B summarizes the storage modulus values obtained within the linear viscoelastic region (LVR) at 1 Hz with 0.2% strain. It was found that hydrogels containing a higher proportion of OCNFMA showed increased stiffness compared with pure ChiMA and formulations containing a lower proportion of OCNFMA. The enhanced crosslinking density induced by methacrylated groups can be attributed to the reinforcing effect of cellulose nanofibers.

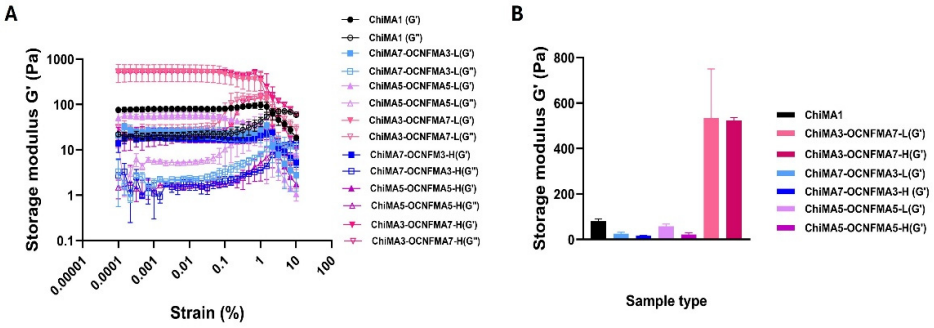

Figure 3. Rheological characterization of hydrogels. (A) Amplitude sweep curves of ChiMA, ChiMA7–OCNFMA3–L, ChiMA5–OCNFMA5–L, ChiMA3–OCNFMA7–L, ChiMA7–OCNFMA3–H, ChiMA5–OCNFMA5–H, and ChiMA3–OCNFMA7–H. (B) Storage modulus (G′), representing the mechanical stiffness of selected hydrogels, obtained from amplitude sweep measurements at 1 Hz frequency and 0.2% strain.

Swelling and degradation are critical indicators of performance and are key factors considered in the design of hemostatic hydrogel systems[1,2,4]. Figure 4A,B show the swelling behavior of the ChiMA and ChiMA-OCNFMA composites over a period of 48 hours in PBS. ChiMA, which exhibited the highest swelling ratio of ~1263 ± 181 at 1 h, appeared to have a highly porous structure in both surface and cross-sectional images, consistent with its high water uptake capacity. The swelling ratio reached 1805 ± 195 and 1844 ± 278 after 4 and 24 hours of incubation in PBS, respectively, indicating that the hydrogel absorbed approximately 18 times its dry weight in water. The incorporation of OCNFMA-L into the ChiMA network at weight ratios of 5:5 and 3:7 (ChiMA:OCNFMA) led to the formation of a highly porous matrix with pore sizes similar to those of pure ChiMA. The composite hydrogel ChiMA3-OCNFMA7-L exhibited a higher swelling ratio (622 + 95% at 1h) than the other formulations during the first hour of immersion in PBS. This behavior can be attributed to the larger pore size of the scaffold, which facilitates water absorption. In contrast, ChiMA3-OCNFMA7-H exhibited a relatively lower swelling ratio (375 ± 95%) compared to ChiMA3-OCNFMA7-L (622 ± 95% at 1h), which may be attributed to its denser structure and relatively smaller pore size. After 48 hours of immersion in PBS, the hydrogel ChiMA3-OCNFMA7-L exhibited a higher swelling ratio (618 ± 20%) than ChiMA3-OCNFMA7-H, which exhibited a value of 565 ± 67%. Due to the lower degree of methacrylation in OCNFMA-L, a more open and porous network structure results, promoting greater water absorption[9]. The higher degree of methacrylation in OCNFMA-H may result in a more

 doi:10.20944/preprints202603.1038.v1

compact matrix and a higher density of crosslinking, which may limit the rate of water absorption over time[9].

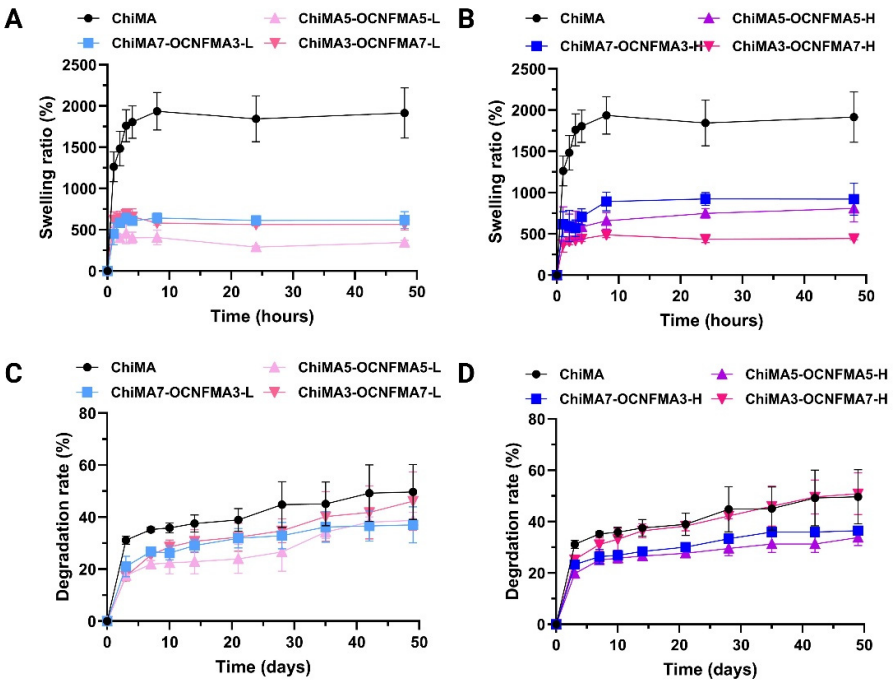

Figure 4. Swelling behavior of ChiMA and its blends with OCNFMA at different weight ratios in PBS:: (A) ChiMA, ChiMA7-OCNFMA3-L, ChiMA5-OCNFMA5-L, and ChiMA3-OCNFMA7-L; (B) ChiMA, ChiMA7-OCNFMA3-H, ChiMA5-OCNFMA5-H, and ChiMA3-OCNFMA7-H measured at 1, 2, 3, 4, 8, 24, and 48 hours. Degradation behavior of the same samples in PBS: (C) ChiMA, ChiMA7-OCNFMA3-L, ChiMA5-OCNFMA5-L, and ChiMA3-OCNFMA7-L; (D) ChiMA, ChiMA7-OCNFMA3-H, ChiMA5-OCNFMA5-H, and ChiMA3-OCNFMA7-H, evaluated over 3, 7, 10, 14, 21, 28, 35, 42, and 49 days.

The biodegradability of biomaterials plays an important and crucial role in tissue engineering[4,9]. It can also be beneficial to control the delivery rate of the therapeutic agent and thereby improve its potency in tissue engineering. The rate of degradation and overall stability of polymeric materials are significantly influenced by both chemical and physical crosslinking [25]. Biopolymers like gelatin, hyaluronic acid, silk fibrin, and chitosan are methacrylated to make them stronger and more resistant to degradation than they would be in their natural state[26]. Polymer degradation is influenced by several factors, including the intrinsic properties of the polymer, the local environment, such as pH, ionic strength, and enzyme concentration, and the presence and type of surrounding cells in the body [9]. Furthermore, the polymer's structural properties, such as its density and porosity, have a big impact on how it degrades[1,9]. Analyses of in vitro degradation can help plan future in vivo experiments and offer important insights into how biomaterials will behave in vivo. Figure 4C,D illustrate the degradation percentages of ChiMA and ChiMA-OCNFMA blend hydrogels with different ChiMA:OCNFMA weight ratios (7:3, 5:5, and 3:7), containing either OCNFMA-L or OCNFMA-H. It can be seen that ChiMA has shown highest degradation among the hydrogen for 7 days, approximately 31 ± 1.51%. by incorporation of the OCNFMA-L the degradation rate slightly decreased.

The introduction of OCNFMA had a significant effect on the degradation behavior of the hydrogels, which was influenced by both the degree of oxidation and subsequent methacrylation and the weight ratio of ChiMA:OCNFM. Among the formulations tested, ChiMA5-OCNFMA5-H, ChiMA5-OCNFMA5-L, ChiMA7-OCNFMA3-H, and ChiMA7-OCNFMA3-L demonstrated

 doi:10.20944/preprints202603.1038.v1

improved stability over time in comparison to composites such as ChiMA3-OCNFMA7-H and ChiMA3-OCNFMA7-L. This improved stability may be due to the higher percentage of ChiMA in these formulations, which likely provides a more cohesive matrix for effective integration and binding of OCNFMA fibers. In contrast, formulations with higher OCNFMA percentages and lower ChiMA percentages may lack sufficient polymer matrix to support adequate fiber entanglement and network formation. As a result, in formulations with lower ChiMA content, the limited amount of matrix material may be hydrolyzed and degraded more rapidly, resulting in the detachment and subsequent degradation of OCNFMA fibers that are no longer held together in the matrix. In contrast, formulations with higher OCNFMA content and lower ChiMA content may lack sufficient polymer matrix to support adequate fiber entanglement and network formation. After 7 days, pure ChiMA exhibited ~35.2% degradation, while composites such as ChiMA7-OCNFMA3-H and ChiMA5-OCNFMA5-H showed lower rates of 26.4% and 25.1%, respectively. Similarly, ChiMA7-OCNFMA3-L and ChiMA5-OCNFMA5-L showed reduced degradation of 27.7% and 17.5%, which indicates improved short-term stability compared to pure ChiMA. By day 49, ChiMA reached ~49.7% degradation, while ChiMA7-OCNFMA3-H and ChiMA5-OCNFMA5-H showed 36.5% and 33.9% degradation, respectively. ChiMA7-OCNFMA3-L and ChiMA5-OCNFMA5-L also remained more stable than pure ChiMA, with degradation values of 37.1% and 39.1%, respectively. However, ChiMA3-OCNFMA7-H and ChiMA3-OCNFMA7-L, which contain the lowest amount of ChiMA, showed degradation values of 33.9% and 17.2% in 7 days, respectively. Notably, ChiMA3-OCNFMA7-H and ChiMA3-OCNFMA7-L showed the highest degradation rates among the composites, reaching 50.9% and 46.2% by day 49, which closely approach or even exceed the degradation observed for pure ChiMA.

BCI is a parameter commonly used to evaluate the hemostatic performance of biomaterials, since it indicates the ability of a material to promote rapid blood coagulation. Low BCI values indicate faster clot formation and, therefore, better hemostatic activity. Figure 5 illustrates the measurement of blood clotting ability of the hydrogels at different incubation times (60–150 s). During the experiment, the negative control (NC) maintained BCI values close to 100%, indicating minimal clot formation, whereas the positive control (PC) displayed lower values due to rapid coagulation. The BCI value for pure ChiMA was approximately 50–55% over the tested time period. The incorporation of OCNFMA significantly affected the clotting behavior of the hydrogels. Among composites containing OCNFMA-L, BCI values decreased with increasing content of OCNFMA, with ChiMA3–OCNFMA7-L showing the lowest value. Hydrogels containing OCNFMA-H also showed a similar trend, with higher OCNFMA content resulting in lower BCI values over time. Hydrogels with higher OCNFMA fractions exhibited lower BCI values than pure ChiMA, suggesting that blood clotting was improved.

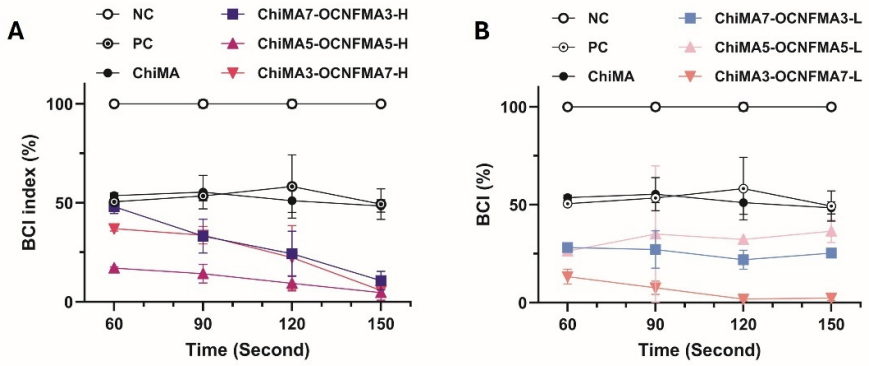

Figure 5. This is a figure. Schemes follow another format. If there are multiple panels, they should be listed as: (**a**) Description of what is contained in the first panel; (**b**) Description of what is contained in the second panel. Figures should be placed in the main text near to the first time they are cited.

 doi:10.20944/preprints202603.1038.v1

Staphylococcus aureus (SA, Gram-positive) and *Pseudomonas aeruginosa* (PA, Gram-negative) are two of the most common bacteria found in chronic wounds and often appear together in the same infected area, making treatment more difficult [12–14]. It has been shown that *PA* and *SA* infections together can be more virulent or worsen patient outcomes than infections caused solely by these bacteria. Both are well known for their resistance to antibiotics. As shown in Figure 6A, a measurable inhibition zone was observed in the hydrogels ChiMA3-OCNFMA7-L, ChiMA3-OCNFMA7-H, and ChiMA5-OCNFMA5-H against SA. As shown in Figure 6B, only the ChiMA3-OCNFMA7-H, ChiMA5-OCNFMA5-H and ChiMA3-OCNFMA7-L, and hydrogels exhibited inhibition zones against SA, measuring 13 mm, 10 mm, and 10 mm, respectively. For PA, the inhibition zones observed for ChiMA3-OCNFMA7-L and ChiMA3-OCNFMA7-H were 11 mm and 10 mm, respectively, while no inhibition was detected for the other samples (Figure 6C). In this case, the methacrylation level of the hydrogel is likely to be the cause of the antibacterial activity. It appears that the presence of OCNFMA contributes to the antibacterial properties of these formulations since OCNFMA is present in a higher weight percentage than ChiMA. In addition, hydrogels containing highly methacrylated OCNFMA-H demonstrated stronger antibacterial effects. In spite of its balanced ratio, ChiMA5-OCNFMA5-H exhibited slight antibacterial activity, suggesting that a higher degree of methacrylation in the OCNFMA component enhances its antibacterial properties. This effect may be attributed to the type of methacrylation agent used in the production of OCNFMA and the resulting chemical structure of the final material. According to the materials synthesis section and illustrated in Scheme 1 , AEMA was used as the methacrylation agent. Several studies have shown that AEMA is capable of imparting antibacterial properties to polymer films [27,28]. There is a possibility that ethanol and methacrylic anhydride may be released during the hydrolysis of the ChiMA-OCNFMA composite. As ethanol possesses antibacterial properties, methacrylic anhydride has the potential to lower the pH locally, thereby creating an unfavorable environment for bacterial growth. These effects may contribute to the antibacterial properties of the hydrogel and influence its ability to inhibit bacterial growth.

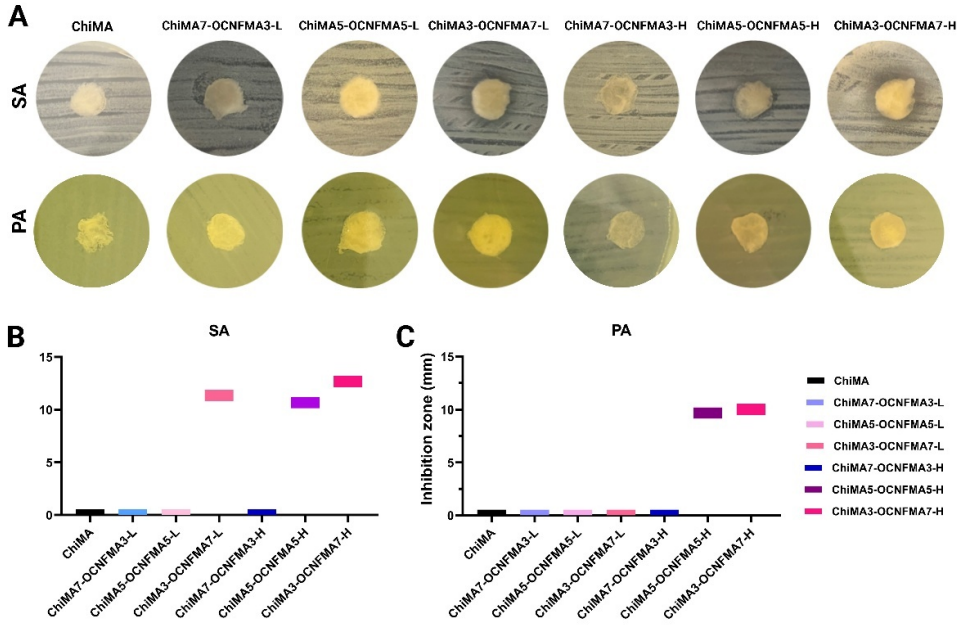

Figure 6. (A) Representative images of ChiMA, ChiMA–OCNFM-(L), and ChiMA–OCNFM-(H) hydrogels against Staphylococcus aureus (SA), Pseudomonas aeruginosa (PA). Inhibition zones of each hydrogel type against (B) SA and (C) PA.

In this study, two types of cells were used to evaluate the interaction between biomaterials and tissue: NIH3T3 fibroblasts, representing soft tissue response in wound healing and hemostasis [29],

 doi:10.20944/preprints202603.1038.v1

and MC3T3 preosteoblasts, representing bone tissue response in the context of bone repair and hemostasis [30]. To assess cytocompatibility, live/dead cell assays were performed to examine the effect of hydrogel leachables on both cell types. As shown in Figure 7, ChiMA alone exhibited low cytocompatibility with NIH3T3 cells, showing approximately 25 ± 20% live cells and 23 ± 8% dead cells, indicating a significant cytotoxic effect. However, after incorporating OCNFMA into the ChiMA network, all composite hydrogels demonstrated improved performance, with cell viability exceeding 70%. This enhancement suggests that the inclusion of OCNFMA increases hydrogel stability and reduces the release of harmful byproducts. Among the composites, those containing highly methacrylated OCNFMA-H showed slightly lower viability than those with OCNFM-L, indicating that a higher degree of methacrylation may negatively influence cell compatibility.

A similar trend was observed in MC3T3 preosteoblasts, where ChiMA alone showed a moderate cytotoxic effect with a cell viability of 63.7 ± 30.5%. In contrast, all ChiMA–OCNFMA composites significantly improved cell viability, further confirming their biocompatibility. The increased number of viable cells in contact with the composite hydrogels may be attributed to the presence of bioactive leachables and cellulose nanofibers, which together create a more favorable microenvironment for bone-like cell attachment and proliferation. Previous studies have demonstrated that the incorporation of cellulose nanofibers can enhance both cell viability and proliferation. Additionally, work by Shukul et al. reported that a higher degree of methacrylation in hydrogel networks can promote the growth of human osteoblasts, likely due to the resulting structural stability and controlled degradation profile, which may release beneficial byproducts.

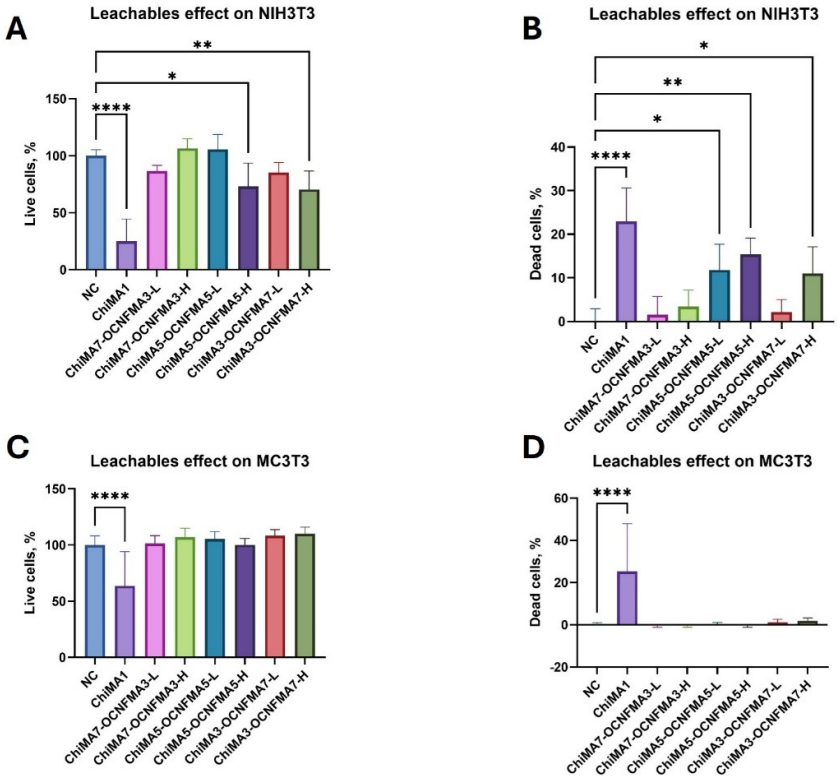

Figure 7. Evaluation of cytotoxicity based on the effect of leachables from hydrogel materials on NIH3T3 fibroblasts and MC3T3 preosteoblasts. **(A)** Percentage of live NIH3T3 cells after exposure to leachates. **(B)** Percentage of dead NIH3T3 cells after exposure to leachates. **(C)** Percentage of live MC3T3 cells after exposure to leachates. **(D)** Percentage of dead MC3T3 cells after exposure to leachates. Data are presented as mean ± SD. Statistical significance was assessed using one-way ANOVA (*p < 0.05, **p < 0.01, ***p < 0.001, ****p < 0.0001).

 doi:10.20944/preprints202603.1038.v1

As shown in Figure 8, in situ crosslinking and injectability of the hydrogel system were evaluated with the custom dual-syringe device. By using this device, ChiMA/LAP solution and OCNFMA dispersion were co-extruded and homogeneously mixed via the static mixing nozzle during manual extrusion. Upon depositing the mixed precursor solution directly on the substrate, the mixture was exposed to UV irradiation (365 nm), resulting in rapid in situ photocrosslinking and the formation of stable hydrogels. Based on these results, the developed hydrogel system can be conveniently delivered using a dual-syringe configuration, which permits efficient hydrogel formation in situ.

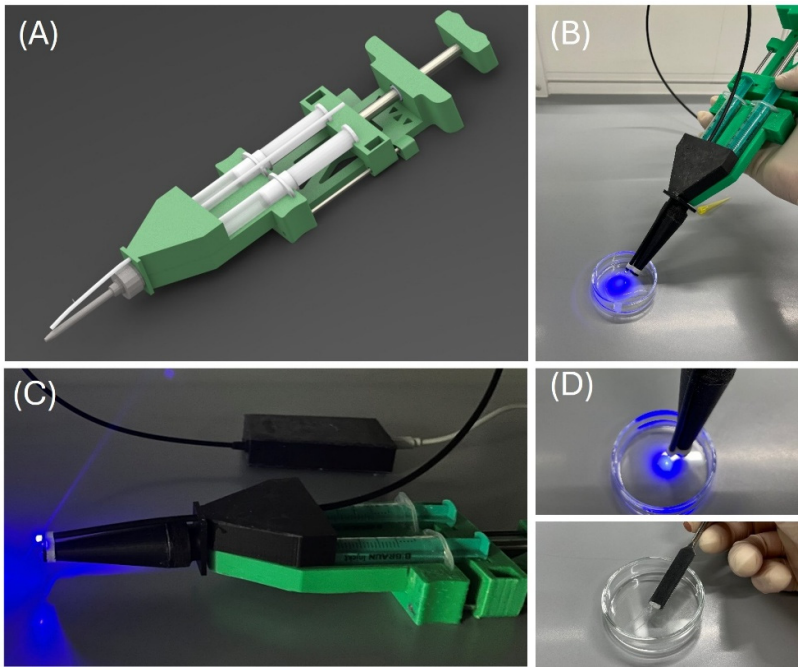

Figure 8. Dual-syringe extrusion system for injectable hydrogel formation. (A) CAD design of the custom dual-syringe device created in SOLIDWORKS. (B) Experimental setup showing simultaneous extrusion of the precursor solutions using the dual-syringe device. (C) UV-assisted photocrosslinking of the extruded hydrogel using a 365 nm light source. (D) Formation of the hydrogel after in situ photocrosslinking and subsequent handling of the crosslinked hydrogel sample.

4. Conclusions

In this study, composite hydrogels based on ChiMA and OCNFMA were successfully developed and characterized. ChiMA-OCNFMA compositions were investigated for their effect on structural, rheological, swelling, and degradation properties of hydrogels. Hydrogel network mechanical stability and structural integrity were improved with the introduction of methacrylate groups. Following UV irradiation, covalent crosslinking occurs between the methacrylate groups. This results in stable composite hydrogel networks. OCNFMA provided a reinforcing effect due to the presence of cellulose nanofibers and enabled tuning of the network structure with a ChiMA:OCNFMA ratio (3:7). The composite hydrogels displayed interconnected porous structures, increased stiffness, and controlled swelling and degradation behavior. Additionally, several formulations demonstrated antibacterial activity against SA and PA, while NIH3T3 and MC3T3 cells showed favorable viability. These results suggest that ChiMA-OCNFMA composite hydrogels are promising multifunctional biomaterials for hemostatic wound management.

Author Contributions: "Conceptualization, J.A. and E.A.Z. ; methodology, J.A., and E.A.Z.; software, J.A, and E.A.Z.; validation, J.A., and E.A.Z.; formal analysis, J.A.; investigation, J.A.,E.A.Z, A.S. and I.S.; resources, J.A,

 doi:10.20944/preprints202603.1038.v1

A.B., D.B. A.S, and I.S.; data curation, J.A.; writing—original draft preparation, J.A.; writing—review and editing, J.A.; visualization, J.A.; supervision, J.A., A.B., and D.B.; project administration, J.A., A.B., and D.B.; funding acquisition, J.A., A.B., and D.B. All authors have read and agreed to the published version of the manuscript.".

Funding: This project has received funding from the European Union's Horizon 2020 research and innovation programme under the grant agreement No. 857287 (BBCE—Baltic Biomaterials Centre of Excellence).

References

1. J. Amirian, Y. Zeng, M.I. Shekh, G. Sharma, F.J. Stadler, J. Song, B. Du, Y. Zhu, In-situ crosslinked hydrogel based on amidated pectin/oxidized chitosan as potential wound dressing for skin repairing, Carbohydrate Polymers 251 (2021) 117005.
2. A.A. Shefa, J. Amirian, H.J. Kang, S.H. Bae, H.-I. Jung, H.-j. Choi, S.Y. Lee, B.-T. Lee, In vitro and in vivo evaluation of effectiveness of a novel TEMPO-oxidized cellulose nanofiber-silk fibroin scaffold in wound healing, Carbohydrate Polymers 177 (2017) 284-296.
3. M.I. Shekh, J. Amirian, F.J. Stadler, B. Du, Y. Zhu, Oxidized chitosan modified electrospun scaffolds for controllable release of acyclovir, International Journal of Biological Macromolecules 151 (2020) 787-796.
4. K. Alizadeh, Y. Dezvare, S. Kamyab, J. Amirian, A. Brangule, D. Bandere, Development of Composite Sponge Scaffolds Based on Carrageenan (CRG) and Cerium Oxide Nanoparticles (CeO2 NPs) for Hemostatic Applications, Biomimetics, 2023.
5. J. Amirian, J.K. Wychowaniec, E. Amel Zendehdel, G. Sharma, A. Brangule, D. Bandere, Versatile Potential of Photo-Cross-Linkable Silk Fibroin: Roadmap from Chemical Processing Toward Regenerative Medicine and Biofabrication Applications, Biomacromolecules 24(7) (2023) 2957-2981.
6. A. Bachhar, P. Dalapati, A. Bose, S. Barman, D. Roy, S. Mandal, Intelligent Self-Healing Hydrogels: AI-Empowered Design, Biomedical Innovation, and Future Horizons, Journal of Drug Delivery Science and Technology (2026) 108215.
7. Y. Qi, F. Wang, J. Liu, C. Wang, Y. Liu, Enzyme-mediated hydrogelation for biomedical applications: A review, International Journal of Biological Macromolecules 311 (2025) 143379.
8. B. Elham, M. Hosseini, M. Mohajer, S. Hassanzadeh, S. Saghati, J. Hilborn, M. Khanmohammadi, Enzymatic Crosslinked Hydrogels for Biomedical Application, Polymer Science, Series A 63(1) (2021) S1-S22.
9. J. Amirian, J.K. Wychowaniec, M. D'Este, A.J. Vernengo, A. Metlova, A. Sizovs, A. Brangule, D. Bandere, Preparation and Characterization of Photo-Cross-Linkable Methacrylated Silk Fibroin and Methacrylated Hyaluronic Acid Composite Hydrogels, Biomacromolecules 25(11) (2024) 7078-7097.
10. H. Kim, J.H. Jeong, M. Fendereski, H.-S. Lee, D.Y. Kang, S.S. Hur, J. Amirian, Y. Kim, N.T. Pham, N. Suh, N.S. Hwang, S. Ryu, J.K. Yoon, Y. Hwang, Heparin-Mimicking Polymer-Based In Vitro Platform Recapitulates In Vivo Muscle Atrophy Phenotypes, International Journal of Molecular Sciences, 2021.
11. A. Sarker, J. Amirian, Y.K. Min, B.T. Lee, HAp granules encapsulated oxidized alginate–gelatin–biphasic calcium phosphate hydrogel for bone regeneration, International Journal of Biological Macromolecules 81 (2015) 898-911.
12. I. Skadiņš, K.D. Labsvārds, A. Grava, J. Amirian, L.E. Tomsone, J. Ruško, A. Viksna, D. Bandere, A. Brangule, Antimicrobial and Antibiofilm Properties of Latvian Honey against Causative Agents of Wound Infections, Antibiotics, 2023.
13. R.H.F. Bashabsheh, O. Al-Fawares, I. Natsheh, R. Bdeir, R.O. Al-Khreshieh, H.H.F. Bashabsheh, Staphylococcus aureus epidemiology, pathophysiology, clinical manifestations and application of nano-therapeutics as a promising approach to combat methicillin resistant Staphylococcus aureus, Pathog Glob Health 118(3) (2024) 209-231.
14. S. Qin, W. Xiao, C. Zhou, Q. Pu, X. Deng, L. Lan, H. Liang, X. Song, M. Wu, Pseudomonas aeruginosa: pathogenesis, virulence factors, antibiotic resistance, interaction with host, technology advances and emerging therapeutics, Signal Transduct Target Ther 7(1) (2022) 199.

 doi:10.20944/preprints202603.1038.v1

15. G.I. Edo, W. Ndudi, A.B.M. Ali, E. Yousif, K. Zainulabdeen, P.O. Akpoghelie, E.F. Isoje, U.A. Igbuku, R.A. Opiti, A.E. Athan Essaghah, D.S. Ahmed, H. Umar, A.A. Alamiery, Chitosan: An overview of its properties, solubility, functional technologies, food and health applications, Carbohydrate Research 550 (2025) 109409.
16. J. Zeng, Z. Zeng, Z. Cheng, Y. Wang, X. Wang, B. Wang, W. Gao, Cellulose nanofibrils manufactured by various methods with application as paper strength additives, Scientific Reports 11(1) (2021) 11918.
17. S. Antony Jose, N. Cowan, M. Davidson, G. Godina, I. Smith, J. Xin, P.L. Menezes, A Comprehensive Review on Cellulose Nanofibers, Nanomaterials, and Composites: Manufacturing, Properties, and Applications, Nanomaterials, 2025, p. 356.
18. Z. Lu, H. Zhang, M. Toivakka, C. Xu, Current progress in functionalization of cellulose nanofibers (CNFs) for active food packaging, International Journal of Biological Macromolecules 267 (2024) 131490.
19. J. Fernández-Santos, C. Valls, O. Cusola, M.B. Roncero, Periodate oxidation of nanofibrillated cellulose films for active packaging applications, International Journal of Biological Macromolecules 267 (2024) 131553.
20. M.E. Lamm, K. Li, D. Ker, X. Zhao, H.E. Hinton, K. Copenhaver, H. Tekinalp, S. Ozcan, Exploiting chitosan to improve the interface of nanocellulose reinforced polymer composites, Cellulose 29(7) (2022) 3859-3870.
21. A. Bucciarelli, N. Selicato, C. Coricciati, A. Rainer, A.L. Capodilupo, G. Gigli, L. Moroni, A. Polini, F. Gervaso, Modelling methacrylated chitosan hydrogel properties through an experimental design approach: from composition to material properties, Journal of Materials Chemistry B 12(40) (2024) 10221-10240.
22. O.M. Kolawole, W.M. Lau, V.V. Khutoryanskiy, Methacrylated chitosan as a polymer with enhanced mucoadhesive properties for transmucosal drug delivery, International Journal of Pharmaceutics 550(1) (2018) 123-129.
23. S. Sayyar, S. Gambhir, J. Chung, D.L. Officer, G.G. Wallace, 3D printable conducting hydrogels containing chemically converted graphene, Nanoscale 9(5) (2017) 2038-2050.
24. X. Zhao, B. Guo, H. Wu, Y. Liang, P.X. Ma, Injectable antibacterial conductive nanocomposite cryogels with rapid shape recovery for noncompressible hemorrhage and wound healing, Nature Communications 9(1) (2018) 2784.
25. A.I. Visan, G. Popescu-Pelin, G. Socol, Degradation Behavior of Polymers Used as Coating Materials for Drug Delivery-A Basic Review, Polymers (Basel) 13(8) (2021).
26. M.C. Catoira, L. Fusaro, D. Di Francesco, M. Ramella, F. Boccafoschi, Overview of natural hydrogels for regenerative medicine applications, Journal of Materials Science: Materials in Medicine 30(10) (2019) 115.
27. K. Wojciechowski, M. Gutarowicz, J. Mierzejewska, P. Parzuchowski, Antimicrobial films of poly(2-aminoethyl methacrylate) and its copolymers doped with TiO2 and CaCO3, Colloids and Surfaces B: Biointerfaces 185 (2020) 110605.
28. A. Punia, P.R. Debata, P. Banerjee, N.-L. Yang, Structure–property relationships of antibacterial amphiphilic polymers derived from 2-aminoethyl acrylate, RSC Advances 5(115) (2015) 95300-95306.
29. X. Lyu, F. Cui, H. Zhou, B. Cao, X. Zhang, M. Cai, S. Yang, B. Sun, G. Li, 3D co-culture of macrophages and fibroblasts in a sessile drop array for unveiling the role of macrophages in skin wound-healing, Biosensors and Bioelectronics 225 (2023) 115111.
30. J. Amirian, N.T.B. Linh, Y.K. Min, B.-T. Lee, The effect of BMP-2 and VEGF loading of gelatin-pectin-BCP scaffolds to enhance osteoblast proliferation, Journal of Applied Polymer Science 132(2) (2015).